International Journal of Nanomedicine

Dovepress
open access to scientific and medical research

Open Access Full Text Article

ORIGINAL RESEARCH

Bioactive Nanoliposomes for Enhanced Sonodynamic-Triggered Disulfidptosis-Like Cancer Cell Death via Lipid Peroxidation

Hongwei Xiang*, Bin Shen*, Chunmei Zhang, Rui Li

Department of Ultrasound, The Third Affiliated Hospital of Chongqing Medical University, Chongqing, People's Republic of China

*These authors contributed equally to this work

Correspondence: Rui Li, Email raylee7991@hospital.cqmu.edu.cn

Introduction: Cell death regulation holds a unique value in the field of cancer therapy. Recently, disulfidptosis has garnered substantial scientific attention. Previous studies have reported that sonodynamic therapy (SDT) based on reactive oxygen species (ROS) can regulate cancer cell death, achieving an limited anti-cancer effect. However, the integration of SDT with disulfidptosis as an anti-cancer strategy has not been extensively developed. In this study, we constructed an artificial membrane disulfidptosis sonosensitizer, specifically, a nanoliposome (SC@lip) coated with a combination of the chemotherapy medicine Sorafenib (Sora) and sonosensitizer Chlorin e6 (Ce6), to realize a one-stop enhanced SDT effect that induces disulfidptosis-like cancer cell death.

Methods: Sorafenib and Ce6 were co-encapsulated into PEG-modified liposomes, and SC@Lip was constructed using a simple rotary evaporation phacoemulsification method. The cell phagocytosis, ROS generation ability, glutathione (GSH) depletion ability, lipid peroxidation (LPO), and disulfidptosis-like death mediated by SC@Lip under ultrasound (US) irradiation were evaluated. Based on a 4T1 subcutaneous tumor model, both the in vivo biological safety assessment and the efficacy of SDT were assessed.

Results: SC@Lip exhibits high efficiency in cellular phagocytosis. After being endocytosed by 4T1 cells, abundant ROS were produced under SDT activation, and the cell survival rates were below 5%. When applied to a 4T1 subcutaneous tumor model, the enhanced SDT mediated by SC@Lip inhibited tumor growth and prolonged the survival time of mice. In vitro and in vivo experiments show that SC@Lip can enhance the SDT effect and trigger disulfidptosis-like cancer cell death, thus achieving anti-tumor efficacy both in vitro and in vivo.

Conclusion: SC@Lip is a multifunctional nanoplatform with an artificial membrane, which can integrate the functions of sonosensitization and GSH depletion into a biocompatible nanoplatform, and can be used to enhance the SDT effect and promote disulfidptosis-like cancer cell death.

Keywords: disulfidptosis, sonodynamic therapy, reactive oxygen species, liposomes, lipid peroxidation

Introduction

Cell death is a fundamental biological process that usually includes necrotic death, apoptosis, pyroptosis, autophagy, ferroptosis, and disulfidptosis.[1–4] Recently, as a non-apoptotic cell death mechanism, disulfidptosis has garnered significant attention in the field of cancer treatment due to its cytotoxic effect on cancer cells.[5,6] Disulfidptosis is a cell death mode caused by disulfide stress, which is induced by the accumulation of cystine or other disulfides in cells.[5] In general, Nicotinamide adenine dinucleotide phosphate (NADPH) provides reducing power to counteract disulfide stress and maintain cellular homeostasis.[7,8] However, under certain conditions such as oxidative damage or reduced GSH levels, intracellular NADPH is excessively consumed, leading to the accumulation of disulfide compounds. This, in turn, triggers the formation of disulfide bonds between actin cytoskeleton proteins, resulting in the collapse of the actin filament (F-actin) network, ultimately leading to disulfidptosis.[7,9,10] During this process, the accumulation of LPO caused by excessive ROS in cells is considered a sign of NADPH consumption, and the accumulation of cystine is the main

Received: 23 March 2024
Accepted: 26 August 2024
Published: 2 September 2024

factor inducing disulfidptosis.[5,11,12] Therefore, adopting effective strategies to increase the intracellular ROS level in cancer cells to induce disulfidptosis efficiently may provide a promising strategy in anti-cancer research.

In recent years, more and more studies have reported therapeutic methods based on ROS,[13] such as Chemodynamic Therapy (CDT),[14] Photodynamic Therapy (PDT),[15] and SDT[16] for treating different types of cancer. As a non-invasive cancer treatment modality, the mechanism of SDT is still unclear, but it is thought that it maybe related to US-mediated activation of sound-sensitive agents to produce ROS in cancer cells.[17] Compared with PDT, SDT has many advantages, such as being non-invasive and having a higher penetration depth, which provides new opportunities for the traditional treatment of deep tumors.[17] Although a large number of studies have confirmed the feasibility of using SDT in various tumor models, the therapeutic effect of SDT in vivo is still limited.[18] Nanotechnology provides an effective strategy to improve the therapeutic effect of SDT by enhancing ultrasonic cavitation, improving the delivery of sonosensitizers, and regulating the tumor microenvironment (TME).[19,20] Therefore, progress in the field of nanotechnology has increased the application potential of SDT.[16] In addition, the exogenous ROS produced by nano-sonosensitizers in the SDT process can cause lipid peroxidation and then induce cell death.[21,22] Moreover, the integration of SDT and lipid peroxidation injury can bypass the apoptosis pathway and thus overcome the inherent resistance of some tumors to apoptosis. However, this strategy has not been developed to a large extent.

SLC7A11 (soluble carrier family 7, member 11, also known as xCT^-) protein is a key component of the cystine/glutamate amino acid reverse transporter (System Xc^-).[23–25] As a type of cystine transporter, SLC7A11 is used to capture and transport cystine from outside into intracellular matrix.[24,26,27] Researchers found that overexpression of SLC7A11 can trigger disulfide bond stress and subsequent cell death.[7,26,27] In other words, SLC7A11 is the central regulator of disulfidptosis, and as a key regulator, it is responsible for manipulating the input of cystine and the biosynthesis of GSH,[12,24,28] which is considered an electron donor in this process. Generally speaking, GSH is highly concentrated (10 mM) in tumor cells, which is more than four times the concentration in normal cells.[25,29] Elevated GSH levels protect cells from external oxidative stress by maintaining redox balance.[30] Therefore, it is a feasible strategy for cancer therapy to deplete intracellular GSH, promote ROS-induced LPO, and increase intracellular disulfide accumulation, such as cystine. Sorafenib is a multi-targeted anticancer chemotherapy medicine that triggers a cascade reaction involving the regulation of redox reaction and apoptosis in cancer cells.[31,32] In addition, Ce6, as a sonosensitizer with a porphyrin ring structure, is considered to be a highly active oxygen-producing reaction catalyst under US radiation.[33,34] Although many anti-cancer studies based on chemotherapeutic medicine combined with sonosensitizer have been reported, no cases of its regulation of disulfidptosis have been reported yet.

Here, we report an SDT sonosensitizer based on Sorafenib-Ce6 nanoliposome (named SC@Lip), which has strong ROS production ability and induces the overexpression of SLC7A11, leading to disulfidptosis. According to our design, the chemotherapy drug Sorafenib and Ce6 were loaded into nanoliposomes. US irradiation endows SC@Lip with the ability of selective accumulation and deep penetration in tumor tissues. We expect that SC@Lip can achieve the anti-cancer effect of SDT by scavenging GSH and accumulating LPO, while inducing disulfidptosis. In the TME (Figure 1), the constructed Nano-SC@Lip, as a sonosensitizer, produces a large amount of ROS under ultrasonic irradiation, which induces the abundant production of LPO in cells and finally promotes the accumulation of disulfide stress. At the same time, SC@Lip depletes GSH in cells through US irradiation, which greatly increases the expression of SLC7A11 protein in cancer cells. The expression level of SLC7A11 determines the susceptibility of cancer cells to oxidative stress. In other words, the excessive expression of SLC7A11 protein causes tumor cells to suffer from peroxide damage, which leads to the cell's inability to transport cystine and the accumulation of disulfide. With the formation of disulfide bonds, the migration of actin cytoskeleton protein is interrupted, and F-actin contracts and separates from the cell plasma membrane, which eventually leads to disulfidptosis-like cancer death. Our research emphasizes that the synthesized the SC@Lips aim at integrating the function of sonosensitizer and glutathione depletion into a biocompatible nanoplatform, which can be used to enhance SDT effect and promote disulfidptosis-like cancer cell death.

Materials and Methods

Materials and Agents

1,2-dipalmitoyl-sn-glycerol-3-phosphatidylcholine(DPPC),1,2-distearoyl-sn-glycerol-3-phosphoethanolamine-N-[methoxy (polyethylene glycol) −2000 (DSPE-mPEG2000), and cholesterol are from Ruixi Biotechnology (Xi'an,

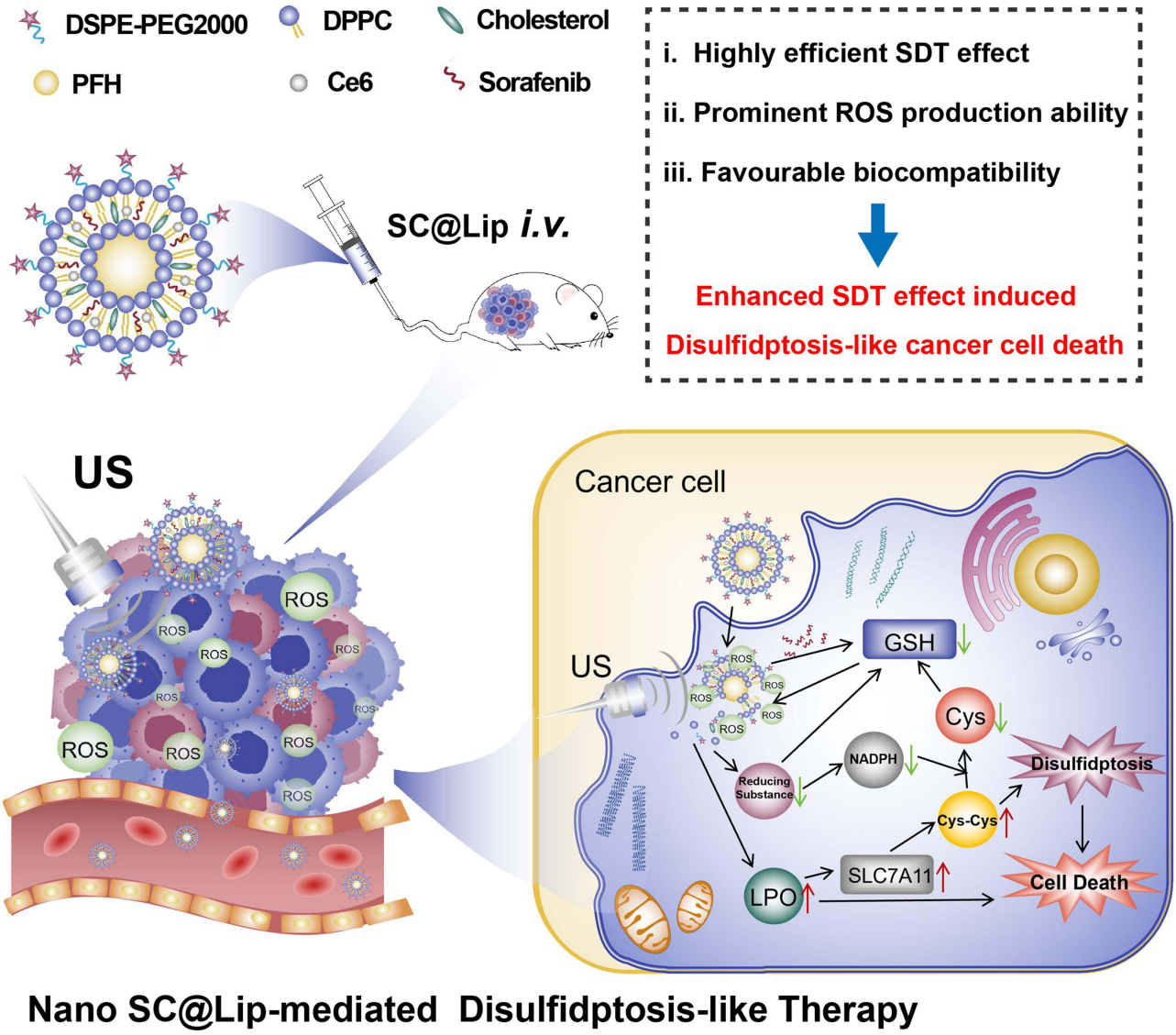

Figure 1 The synthetic components of lipid sonosensitizer -SC@Lip, and the schematic diagram of its mechanism for realizing SDT anticancer effect and inducing disulfidptosis-like cancer cell death.

China). Chloroform was purchased from Chuandong Chemical Co.Ltd. (Chongqing, China). Sorafenib (Sora), Chlorin e6 (Ce6) and Perfluorohexane (PFH) were purchased from Aladdin. (Shanghai, China) 1, 3-diphenylisopropylfuran (DPBF) and methanol were purchased from Macklin Biochemical Co. Ltd. (Shanghai, China). Singlet oxygen sensor green fluorescent probe (SOSG) is from Invitrogen. (California, USA). Phosphate Buffered Saline (PBS), RPMI 1640 medium, 4T1 cell line and 4T1 special medium (CM-0007) was purchased from Procell (Wuhan, China). Calcein-acetoxymethyl ester (Calcein-AM), propidium iodide (PI), 4',6- diamidino-2-phenylindole (DAPI), 2',7'-Dichlorodihydrofluorescein diacetate (DCFH-DA) kit and Actin-Tracker Green-488 were purchased from Beyotime biotechnology. (Shanghai, China). Reduced GSH content detection kit was purchased from Solarbio (Beijing, China). Lipid peroxidation probe-BDP 581/591C11 reagent comes from Dongren Chemical Technology (Shanghai, China). Annexin V-FITC/PI apoptosis detection kit was purchased from 4A Biotech (Suzhou, China). Anti-xct/SLC7A11 mouse monoclonal antibody [A7C6] was purchased from HuaAn Bio. (Hangzhou, China). Goat anti Mouse IgG H&L (Alexa Fluor 555) second antibody was from Abcam (Waltham, the USA).

Synthesis of SC@Lip

SC@Lip was prepared by a simple rotary evaporation phacoemulsification method. In summary, DPPC, DSPE-mPEG 2000, and cholesterol were dissolved in 8 mL chloroform at a weight ratio of 6:2:2. Then, 2 mg of Sorafenib and 2 mg of Ce6 were dissolved in 2 mL methanol and then mixed with the above solution. Then the mixture above was placed in an ultrasonic cleaning machine so that the components were fully dissolved. Next, the mixture was rotary evaporated for 30 minutes to evaporate the chloroform and methanol form a thin green lipid film. After that, PBS was added, and the formed film was peeled off with ultrasonic assistance. Then, PFH (200 μL) was added to the mixture solution, followed by sonication at a power density of 52W (5s on, 5s off) for 5 minutes. After centrifugation (8000 rpm, 5 minutes), the precipitate was collected. As for the preparation of Ce6@Lip or Sora@Lip nanoliposome, the difference lies in the omission of Sorafenib or Chlorin e6. All liposomes are stored in a 4°C refrigerator, closed and dark.

Characterization of SC@Lip

The morphology of the obtained SC@Lip was observed using a transmission electron microscope (TEM, Thermo Fisher Scientific, the USA). The zeta potential and hydrodynamic diameter were measured with a Malvern Zetasizer Nano Series (the UK). UV-Vis-NIR detection was carried out using a microplate reader, SpectraMax M3 (the USA). The drug loading rates and entrapment efficiency rates were tested by High Performance Liquid Chromatography (HPLC), specifically using the SHIMADZU LC-20A machine (Japan).

For ROS detection: Add 1.3-diphenylisobenzofuran (DPBF) solution (final working concentration is (10 mM) into a Ce6@Lip solution (50 μg/mL) in a 6-well plate and mix thoroughly. Next, the mixture was stimulated with an ultrasound therapy instrument, Nu-Tek UT1021 (Shenzhen, China). This instrument was used in all experiments of this study. Ultrasonic parameters were set to 2.0 W/cm^2 1.0 MHz, 50% duty cycle, for 1, 2, 3, 4, and 5 minutes. After that, the absorbance was recorded at 410 nm using an enzyme-labeled instrument. Add Singlet Oxygen Sensor Green Fluorescent Probe (SOSG)solution (final working concentration of is 5 nM) into a Ce6@Lip solution (50 μg/mL), treat the mixture as above, and then use a fluorescence spectrophotometer, Agilent Cary Eclipse 5000 (the USA), to record the fluorescence spectrum of SOSG to detect Singlet Oxygen ($^1O_2$) production.

Cell Culture

Using 4T1 special medium, 4T1 cells were cultured and placed at 37°C in a 5% CO_2 atmosphere. Once high-density logarithmic growth of the cells was observed, they were digested with 0.25% trypsin solution for subsequent use.

Application Proportion of SC@Lip and Ultrasonic Parameter Selection

To select the optimal application ratio of SC@Lip, 4T1 cells were cultured in 6-well plates at a density of 1×10^5 cells per well for subsequent experiments.

In the experiment to determine the optimal ultrasonic actuation time and power. Liposomes were added to a 6-well plate at a drug concentration of 250 μg/mL SC@Lip and incubated with the cells for 12 hours. In particular, all therapeutic liposomes concentrations refer to the concentration of liposomes in this study. Subsequently, the 4T1 cells were treated with ultrasonic actuation time and power gradients: 0 W/cm^2, 0.5 W/cm^2 for 10s, 0.5 W/cm^2 for 30s, 0.5 W/cm^2 for 60s, 1 W/cm^2 for 10s, 1 W/cm^2 for 30s, and 1 W/cm^2 for 60s.

In the experiment to determine the optimal liposome concentrations. SC@Lip were added to the cells in the 6-well plate at the concentration (0 μg /mL, 50 μg/mL, 125 μg/mL, 250 μg/mL, and 500 μg/mL SC@Lip and 250μg/mL empty liposomes, named as Lipo). The incubation time was 12 hours, Then, the 4T1 cells cocultured with SC@lip were irradiated with ultrasound (0.5 W/cm^2, 30s).

Finally, all the cells above were collected simultaneously, stained with Calcein-AM according to the instructions. The calcein-AM reagent was diluted 1000 times volume with PBS and incubated with cells at 37 °C for 30 min protected from light. The cells were then detected by CytoFLEX flow cytometer (Beckman Coulter, USA).

Intracellular Phagocytosis of SC@Lip and It's Therapeutic Effect in vitro

Intracellular phagocytosis of SC@Lip was monitored using a confocal laser scanning microscope (CLSM, Nikon, Japan). 4T1 cells in the logarithmic growth phase were cultured overnight in confocal dishes, and subsequently, the culture medium in each dish was replaced with medium containing SC@Lip (50μg/mL). After various time intervals (0, 2, 4, 8, and 12 hours), the cells were washed with PBS and promptly fixed with 4% paraformaldehyde for 15 minutes. Finally, the nuclei of the 4T1 cells were labeled with DAPI for observation under the CLSM.

To evaluate the in vitro sonodynamic therapeutic effect of SC@Lip, 4T1 cells were inoculated in 6-well plates at a density of 1×10^5 cells per well and cultured overnight. The cells were then divided into six groups: (I) untreated cells (Control), (II) Empty liposomes (Lipo), (III) Sora@Lip, (IV) SC@Lip, (V) Ce6@Lip + US, and (VI) SC@Lip + US, to compare the survival status of cells following different treatments. Cells in groups (II) to (VI) were incubated with nanoliposomes (250μg/mL) for 12 hours. Subsequently, the cells in groups (V) and (VI) were irradiated with ultrasound at 0.5 W/cm^2 for 30 seconds. After treatment, all cells were collected and stained with Annexin V-FITC/PI according to kit instructions to assess the cell survival rate using CytoFLEX flow cytometer (FCM). Additionally, Repeat the above steps, following staining with Calcein-AM/PI (dilution volume ratio is 1:1000), the CLSM was utilized to distinguish dead cells (red fluorescence) from living cells (green fluorescence).

Measurement of ROS, GSH and LPO in Cells After SDT Effect Mediated by SC@Lip

4T1 cells were inoculated into a confocal culture dish for 24 hours and the cells were then divided into six groups: (I) untreated cells (Control), (II) Lipo, (III) Sora@Lip, (IV) SC@Lip, (V) Ce6@Lip + US, and (VI) SC@Lip + US, to compare the survival status of cells with different treatments. Cells in groups (II) to (VI) were incubated with nanoliposomes (250μg/mL) for 12 hours. Subsequently, the cells in groups (V) and (VI) were irradiated with ultrasound (0.5 W/cm^2,30s).

To detect intracellular ROS, the Serum-free -RPMI 1640 medium was supplemented with DCFH-DA reagent (final working concentration of is 10 μM), and the cells in the aforementioned groups were incubated for 30 minutes. Afterward, the fluorescence signal of the cells at 488 nm was detected using CLSM. Furthermore, the fluorescence of DCFH-DA in the cells was also quantified using FCM for quantitative analysis.

To assess the level of GSH consumption in cells, 4T1 cells were seeded in T75 cell culture bottles (2×10^7 cells per bottle) overnight. All the 4T1 cells were then divided into five groups: (I) untreated cells (Control), (II) Sora@Lip, (III) SC@Lip, (IV) Ce6@Lip + US, and (V) SC@Lip + US. Cells in groups (II) to (V) incubated with nanoliposomes (250μg/mL) for 12 hours. Afterward, the cells in group (IV) and (V) were irradiated with ultrasound (0.5 W/cm^2,30s) and then washed three times with PBS, collected, and subjected to ultrasound (200 W, on 3s, off 10s, 30 cycles). The supernatant was then analyzed for GSH levels using HPLC (SHIMADZU LC-20A).

For further intracellular lipid peroxidation (LPO) evaluation, the cells were treated similarly to the ROS detection procedure. Subsequently, the culture medium (dilution volume ratio is 1:1000) was supplemented with Lipid Peroxidation Probe -BDP C11 reagent, and the cells were cultured for 30 minutes. After washing with PBS, the cells were examined under CLSM with excitation/emission wavelengths of 581/591 nm.

Determination of SLC7A11 Protein Expression in Cells and Cell Cytoskeleton After SDT Effect Mediated by SC@Lip

4T1 cells were inoculated into a confocal culture dish for 24 hours and the cells were subsequently divided into six groups: (I) untreated cells (Control), (II) Lipo, (III) Sora@Lip, (IV) SC@Lip, (V) Ce6@Lip + US, and (VI) SC@Lip + US, to compare the SLC7A11 protein expression and cell cytoskeleton in cells following different treatments. Cells in groups (II) to (VI) were incubated with nanoliposomes (250μg/mL) for 12 hours. Subsequently, the cells in groups (V) and (VI) were irradiated with ultrasound (0.5 W/cm^2,30s).

After the treatment, the cells were washed with PBS and immediately fixed with 4% paraformaldehyde for 15 minutes. The cell dishes were then incubated with SLC7A11 antibody (dilution volume ratio is 1:500) overnight. The following day, the cells were incubated with the secondary antibody (dilution volume ratio is 1:1000), abcam IgG H&L (Alexa Fluor 555) at room temperature for 30 minutes. Finally, 4T1 cell nuclei labeled with DAPI, and the 4T1

cytoskeleton protein, F-actin labeled with Actin-Tracker Green-488 (dilution volume ratio is 1:100) for observation under CLSM.

Establishment of Animal Tumor Models

Balb/c female mice (6–8 weeks old) were purchased from the Experimental Animal Center of Chongqing Medical University. All animal procedures adhered to the guidelines of the Animal Care Ethics Committee of Chongqing Medical University (animal welfare ethics approval number: IAUC-CQMU-2024-0016). To establish a subcutaneous breast cancer tumor model, 100 μL of 4T1 cells (1×10^8 cells/mL) were injected subcutaneously into the abdominal region of the mice. Then monitor the size of the tumor everyday.

Evaluations of the Therapeutic Effects Mediated by SC@Lip in vivo

The experiment was conducted in two batches. When the tumor volume reached approximately 100 mm^3, treatment commenced, designated as day 0. Liposomes were injected on days 0, 3, and 6, and ultrasound treatment was administered on days 1, 4, and 7. The dosage was 10 $mg.kg^{-1}$ (nanolipsomes concentration), and the administration route was via tail vein injection. The tumor-bearing mice were randomly divided into five groups (n = 5 per group): I) PBS (Control); II) Sora@Lip; III) SC@Lip; IV) Ce6@Lip + US; V) SC@Lip + US. Following the injection of nanoliposomes, the tumor areas of mice in groups IV and V were exposed to ultrasound irradiation (2 W/cm^2, 3 min). During the follow-up period, the weight and tumor volume of the mice were measured every two days. When the tumor volume exceeded or equaled 1500 mm^3, the follow-up was terminated, and the mice in one batch were euthanized. Tumor tissues were collected, fixed with 4% paraformaldehyde, sent to Ultron Biotechnology Co., LTD (Chengdu, China). H&E staining, immunofluorescence staining (TUNNEL, PCNA) and immunohistochemistry (SLC7A11 protein) were performed after standard operation procedures such as dehydration, embedding, section, dewaxing dehydration, staining, sealing and observed by fluorescence biological microscope MF-23-M (Mshot Photoelectric Technology Co., LTD, Guangzhou, China). The remaining batch continued to measure tumor size to the endpoint for Kaplan-Meier simple survival analysis.

Biosafety Assessment of SC@Lip

Healthy Balb/c mice were treated with SC@Lip (10 $mg.kg^{-1}$) via tail vein injection. Blood samples from the mice were collected at various time points (day 1, 3, 7, 14, and 21) for hematological analysis and biochemical detection. For the control group, mice were treated with 200 μL of PBS using the same administration method. Additionally, the primary organs were submitted and fixed with 4% paraformaldehyde, also sent to Ultron Biotechnology Co., LTD for H&E pathological analysis.

Biological Distribution of Liposomes of SC@Lip

Eighteen Balb/c tumor-bearing mice were randomly divided into 6 groups, with 3 mice in each group. One group served as the control group, while the others were experimental groups. The experimental groups received a tail vein injection with SC@Lip (10 $mg.kg^{-1}$). One group of mice was randomly euthanized at 4, 8, 12, 24, and 30 hours post-injection, respectively. The control group was injected with an equal volume of PBS and then euthanized. The tumor tissues and major organs (heart, liver, spleen, lungs, and kidneys) were completely excised and immediately imaged using an AniView100 Pro fluorescence imaging system (Biolight Biotechnology, Guangzhou, China) for ex vivo tissue fluorescence imaging. Subsequently, quantitative analysis of tissue fluorescence intensity was performed (Ce6 excitation/emission wavelengths: 675/760 nm).

Statistical Analysis

All data are expressed as mean ± standard deviation. Analysis of variance between two or more groups. The data were analyzed according to Tukey's multiple comparisons test. The data is considered significant at $P < 0.05$. The standard symbols are * $p \leq 0.05$, * * $p \leq 0.01$ and * * * $p \leq 0.001$, * * * * $p \leq 0.0001$.

Results and Discussion

Characterization of SC@Lip

SC@Lip was synthesized using rotary evaporation phacoemulsification method. TEM images reveal that the synthesized SC@Lip exhibits a regular and uniform spherical structure (Figure 2A). The prepared SC@Lip is well dispersed and appears as a dark green suspension (Figure 2B). We analyzed the UV-vis spectra of all the components involved in the synthesis of SC@Lip (Figure 2C). Based on the ultraviolet spectra obtained for various concentrations of Sorafenib (Figure S1) and Ce6 (Figure S2), we determined that Sorafenib has a characteristic UV absorption peak at approximately 290 nm, while Chlorin e6 has two characteristic UV absorption peaks at 400 nm and 650 nm, respectively. As is evident from Figure 2D, the spectrum of SC@Lip displays three distinct characteristic bands around 290 nm, 400 nm, and 650 nm, indicating the successful loading of Sorafenib and Chlorin e6.

Using dynamic light scattering (DLS), we measured the average hydrodynamic diameter of SC@Lip to be 258.03 nm ± 0.54 nm (PDI: 0.097 ± 0.06) (Figure 2E), and the surface zeta potential to be approximately 27.2 mV ± 5.99 mV. The stability of SC@Lip was investigated by monitoring the hydrodynamic diameter of the liposomes over time. Figure 2F demonstrates that the size remained largely unchanged within 28 days, indicating that SC@Lip possesses good colloidal stability. In addition, by analyzing the HPLC standard chromatograms of Sorafenib (Figure S3) and Chlorin e6 (Figure S4) at 50 ppm, we determined the optimal detection wavelength (264 nm for sorafenib and 406 nm for Chlorin e6) and retention time (9.8 min for Chlorin e6 and 17.5 min for Sorafenib). Based on these findings, we established the detection method. The HPLC standard curves for Sorafenib was Y=126.246X-2768.03, R2=0.9996 (Figure S5) and for Chlorin E6 was Y=237.512X-14192.9, R2=0.9995 (Figure S6) by analyzing various concentrations of each standard solution. Utilizing these HPLC standard curves for Chlorin E6, we quantified its content in the supernatant. According to the following equation:

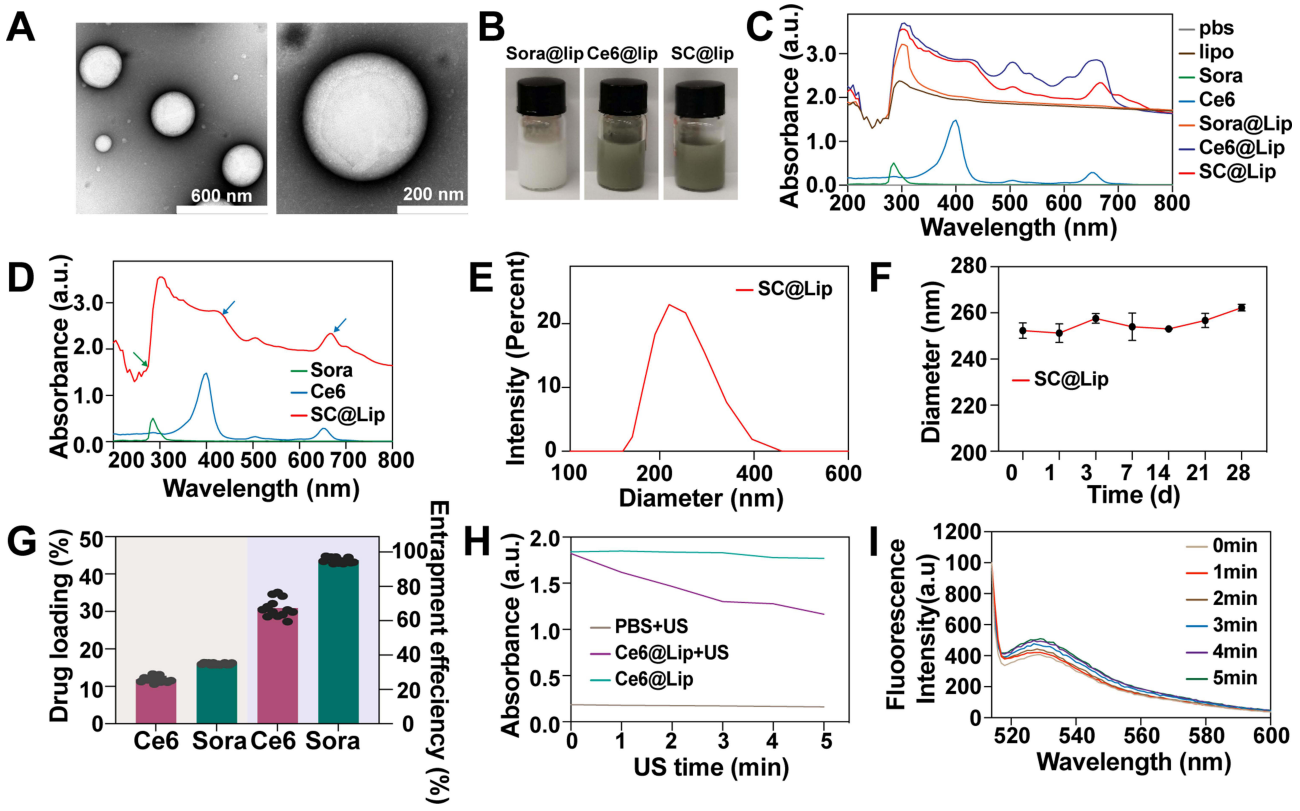

Figure 2 Characterization of SC@Lip. (**A**) TEM image of SC@Lip (scale bar: 600nm, 200 nm). (**B**) Digital photos of Sora@Lip, Ce6@Lip and SC@Lip. (**C**) UV-Vis-NIR absorption spectra of Lipo, Sorafenib, Ce6, Sora@Lip, Ce6@Lip and SC@Lip. **(D)** UV-Vis-NIR absorption spectra of Sorafenib, Ce6, and SC@Lip. (**E**) Hydrodynamic diameter of SC@Lip. (**F**) Hydrodynamic diameter of SC@Lip in 28 days. (**G**) Drug loading rate and entrapment efficiency of Sorafenib and Ce6 in SC@Lip. (**H**) DPBF absorption curve and **(I)** SOSG fluorescence spectrum of SC@Lip under US irradiation.

Encapsulation efficiency = (quality of drug input - quality of drug in supernatant)/quality of drug input x100%

Drug loading = (quality of drug input - quality of drug in supernatant)/total mass of liposomes x100%

We calculated that the loading of Ce6 in SC@Lip liposomes was 11.87% ± 0.1% (w/w), with an encapsulation efficiency (EE) of 67.33% ± 0.2% (Figure 2G). Similarly, we determined the drug loading of Sorafenib to be 16.02% ± 0.09% (w/w), with an EE of 95.35% ± 0.12% (Figure 2G).

Both Ce6 and Sorafenib are hydrophobic drugs with low bioavailability. However, the SC@Lip nanoliposomes exhibit a good encapsulation efficiency for both Sorafenib and Ce6. Their nanosize enables them to penetrate tumors in large quantities through the enhanced permeability and retention (EPR) effect.[35,36,37] To validate the ROS-generating capability of our synthesized liposomes, we conducted relevant experiments using DPBF and the SOSG probe. 1.3-Diphenylisobenzofuran (DPBF) is a fluorescent probe which, for almost 20 years, was believed to react in a highly specific manner toward some reactive oxygen species such as singlet oxygen and hydroxy, alkyloxy or alkylperoxy radicals. After DPBF is irreversibly oxidized by ROS, and the absorbance of UV-visible light at 410 nm is rapidly reduced, which can be used as a ROS indicator.[38] Singlet oxygen is a kind of ROS. when $^1O_2$ reacts with SOSG to form SOSG endoperoxide (SOSG-EP), the internal electron transfer is prevented, and the fluorescence at ex/em 504/525 nm can be increased.[39] As shown in Figure 2H, Ce6@Lip After ultrasonic irradiation, the absorbance of 410 nm showed a significant decreasing trend with the extension of ultrasonic irradiation time, while the absorbance of 410 nm did not decrease significantly without ultrasonic irradiation. After ultrasonic irradiation of PBS, the absorbance of 410 nm showed a basically straight line change. Similarly, the SOSG test analysis revealed analogous results (Figure 2I), Ce6@Lip After ultrasonic irradiation, the fluorescence intensity of SOSG increased with the extension of ultrasonic irradiation time. These findings confirm that Ce6@Lip possesses the ability to generate ROS, thereby further enhancing the efficacy of sonodynamic therapy.

Moreover, nanoliposomes can enhance solubility, permeability, and bioavailability.[40] The above results indicate that we successfully synthesized SC@Lip, which exhibits ROS production capacity. Therefore, it holds potential as a sonosensitizer to amplify SDT's effectiveness and can be utilized in anticancer therapy to achieve more efficient treatment while minimizing side effects.

Application Proportion of SC@Lip and Ultrasonic Parameter Selection

To achieve an efficient and controllable therapeutic effect of SDT, it is crucial to evaluate the application performance of nanoliposomes. Using Calcein-AM FCM, we screened for the optimal concentration of nanoliposomes as well as the optimal ultrasonic power and duration. First we selected a concentration of SC@Lip nanoliposomes (250 μg/mL) as the pretreatment concentration for further experiments to determine the optimal ultrasound parameters (Figure 3A and C).In the SC@Lip + US group, the combination of 0.5 W/cm² and 30s achieved a highly effective tumor-killing effect, resulting in a cell survival rate of only 7% ± 0.8%. Using the selected US parameters (0.5 W/cm², 30s), we further tested the effects of varying liposome concentrations. As anticipated (Figure 3B and D), 4T1 cells incubated with SC@Lip nanoliposomes (250μg/mL) for 12 hours exhibited significant cytotoxicity when stimulated with ultrasound. The survival rate of 4T1 cells was less than 10%, demonstrating excellent cytotoxicity. When 4T1 cells cocultured with 250ug/mL empty liposomes, cells mean viability was 94.6% indicated that our lipid carrier has good biosafety. Based on these findings, using the nanoliposomes (250μg/mL) combined with US (0.5 W/cm², 30s) is a reasonable choice to drive an efficient SDT effect and cancer treatment in subsequent experiments.

Intracellular Phagocytic of SC@Lip and It's SDT Therapeutic Effect in vitro

Encouraged by the optimal SDT effect of SC@Lip, we further investigated its application at the 4T1 cells level. Firstly, we analyzed the intracellular phagocytic of SC@Lip using CLSM. As depicted in Figure 4A, after 2 hours of incubation, SC@Lip began to be internalized by 4T1 tumor cells, evidenced by the presence of Ce6's spontaneous 647 nm red fluorescence. The intracellular red fluorescence gradually increased with the prolongation of incubation time, reaching its peak at 8 hours and maintaining this level until 12 hours. This demonstrates the efficient phagocytic ability of SC@Lip.

Next, we evaluated the therapeutic effect of SC@Lip on SDT by assessing apoptosis through FCM experiments. As depicted in Figure 4B–D, the late apoptosis plus cell debris rates for the Sora@Lip, SC@Lip, and Ce6@Lip + US groups were

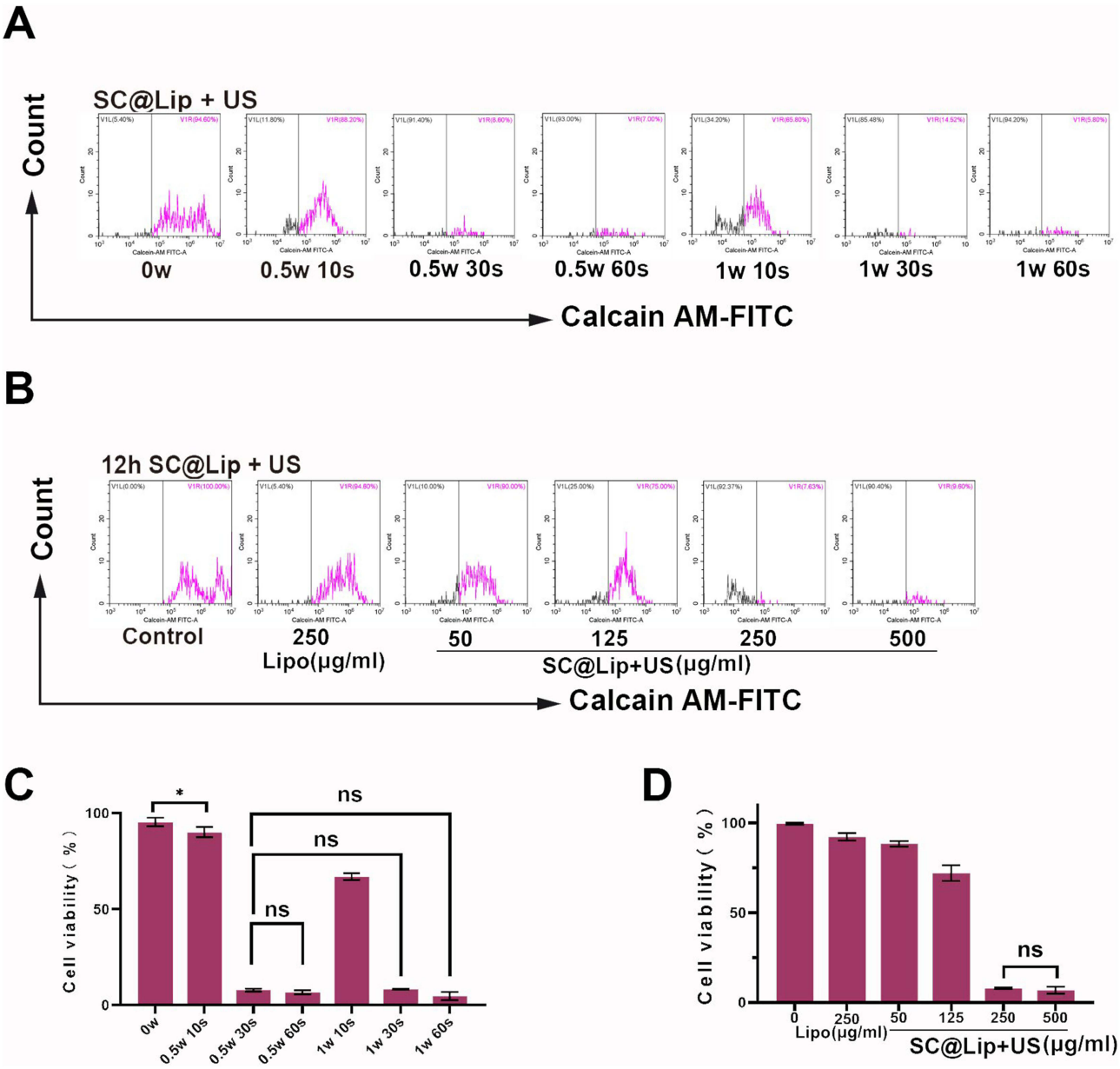

Figure 3 Application proportion of SC@Lip and Ultrasonic Parameter selection. (**A**) The Calcain-AM FCM chart of Ultrasonic Parameter selection. (**B**) The Calcain-AM FCM chart of application proportion of SC@Lip selection. (**C**) Statistical histogram of Ultrasonic Parameter selection. (**D**) Statistical histogram of application proportion of SC@Lip selection. (**ns** means no statistical difference, *p < 0.05).

approximately 81.33% ± 3.42%, 76.17% ± 3.48%, and 86.85% ± 2.83%, respectively. In contrast, the SC@Lip + US group exhibited the most potent cytotoxicity against 4T1 cells, with a late apoptosis plus cell debris rate as high as 93.69% ± 1.85%.

We further utilized Calcein-AM and PI staining to identify living cells (green fluorescence) and dead cells (red fluorescence). As shown in Figure 4E, CLSM images revealed that almost all 4T1 cells treated with the SC@Lip + US group exhibited red fluorescence, indicating severe cell death. This finding is consistent with the Annexin V/PI staining FCM results. As anticipated, SC@Lip liposomes exhibit high phagocytic efficiency and strong toxicity in 4T1 cells. This anti-cancer effect mediated by SC@Lip can reduce the survival rate of cancer cells.

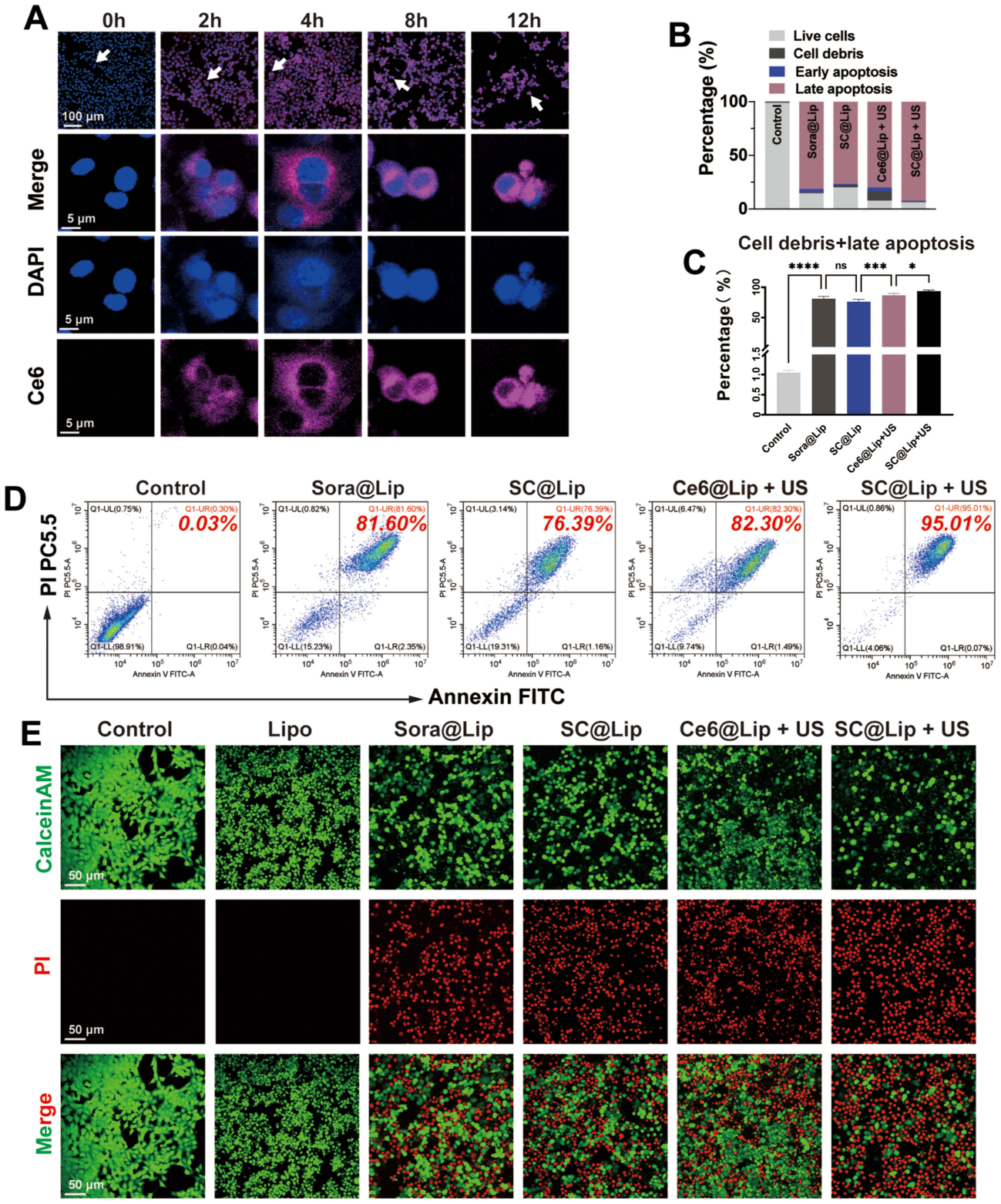

Figure 4 Intracellular phagocytosis of SC@Lip and its SDT therapeutic effect in vitro. (**A**) Intracellular phagocytosis of SC@Lip detected by CLSM (scale bar:100 μm, 5 μm).) (**B**, **C** and **D**) Statistics histograms and FCM data plots showing Annexin V-FITC/PI staining results detected by flow cytometry for evaluating therapeutic effect in vitro after 4T1 cells were treated in each group (n=6). (**E**) CLSM diagram of Calcein AM (green-living cells) /PI (red-dead cells) after 4T1 cells were treated in each group. All experiments were repeated independently at least twice, and the results were similar. (**ns** means no statistical difference, *p < 0.05, ***p < 0.001, ****p < 0.0001).

Measurements of ROS, GSH in Cells After SDT Effect Mediated by SC@Lip

SDT relies on the mechanism where sonosensitizers generate ROS under ultrasonic radiation to combat cancer cells.[41] To assess the potential of our SC@Lip as a sonosensitizer in SDT, evaluating its ability to induce lipid peroxidation and redox imbalance is imperative. Intracellular ROS can oxidize non-fluorescent DCFH to produce fluorescent 2',7'-dichlorofluorescein (DCF). Detecting the fluorescence of DCF can determine the level of intracellular reactive oxygen species. We employed the standard fluorescent probe DCFH-DA to quantify intracellular ROS levels in 4T1 cells following various treatments. As observed in the CLSM images in Figure 5A, 4T1 cells treated with SDT (Ce6@Lip +

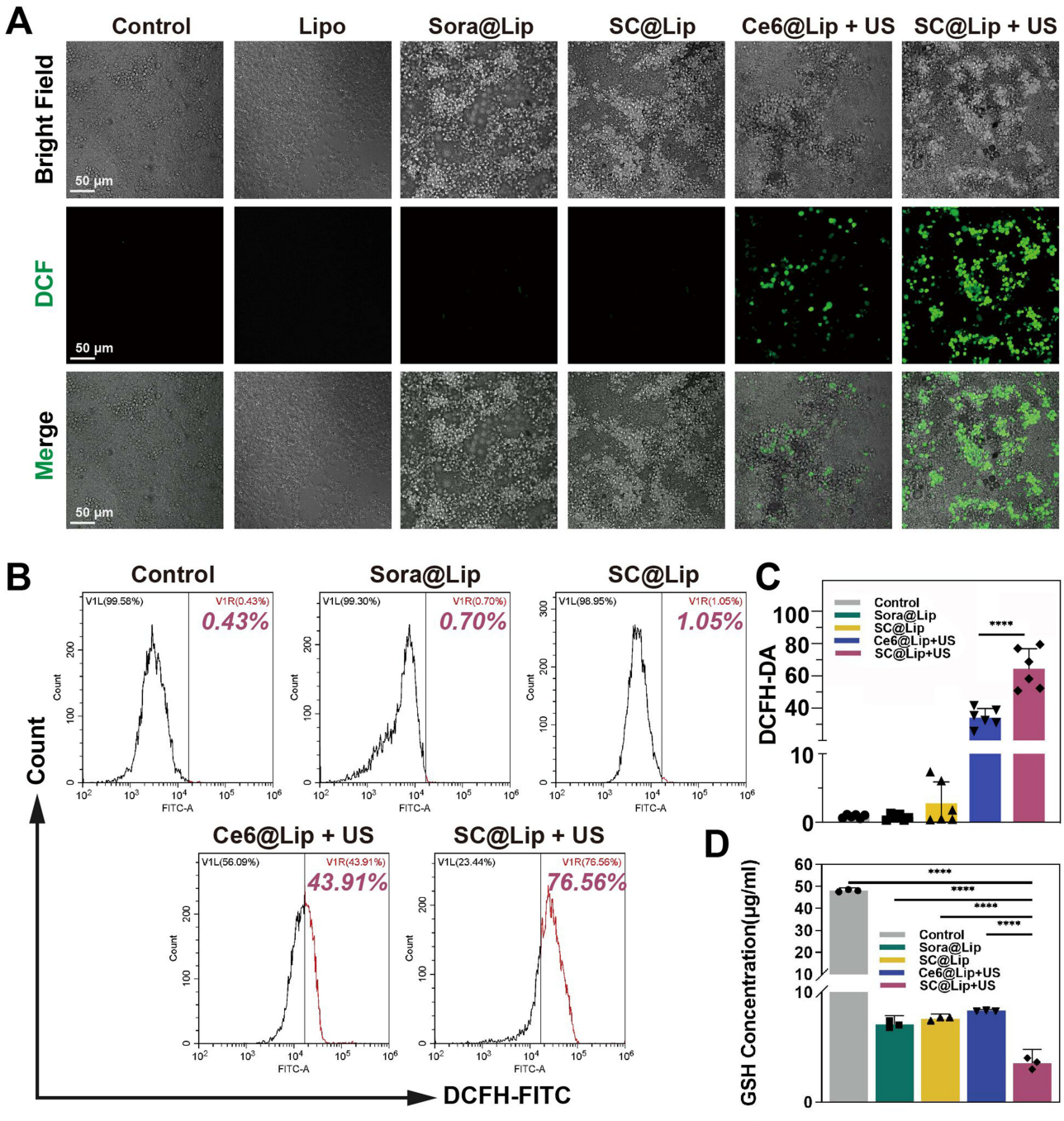

Figure 5 Detection of intracellular ROS and GSH. (**A**) CSLM images of DCFH-DA after 4T1 cells were treated with each group. (scale bar: 50μm) (**B**) FCM charts of DCFH-DA test. (**C**) FCM Statistical histograms (n=6) of DCFH-DA test. (**D**) Detection of GSH content in the cells after 4T1 cells were treated with each group (n=3). The concentration of nanoliposomes was 250μg/mL, and the cells were incubated for 12h. The US parameters of SDT group were 0.5 W/cm^2, 30s. All experiments were repeated independently at least twice, and the results were similar. (****p < 0.0001).

US and SC@Lip + US groups) exhibited green fluorescence signals, while the other four groups did not, indicating that our synthesized SC@Lip nanoliposomes generated ROS in cells under ultrasonic activation.

The DCFH-DA FCM results and their corresponding quantitative data in Figure 5B–C corroborate the findings from the CLSM images. Notably, the SC@Lip group demonstrated the most significant intracellular ROS production effect, attributable to Sorafenib, a multi-kinase inhibitor, which can regulate the redox homeostasis of drug-resistant cancer cells. Glutathione is the primary antioxidant in the cytoplasm.[42] Since glutathione levels in cells are often depleted due to oxidative stress,[43] we utilized HLPC to measure the GSH content in 4T1 cells. As shown in Figure 5D, the intracellular GSH level in the Sora@Lip, SC@Lip, Ce6@Lip + US and SC@Lip + US groups decreased significantly, but SC@Lip + US group was the most obvious ($p<0.01$).

In summary, the high ROS levels and GSH depletion induced by our SC@Lip undoubtedly enhance the SDT effect, highlighting its excellent potential as a sonosensitizer.

SC@Lip Mediates SDT Triggered Intracellular Lipid Peroxidation and Cell Cytoskeleton Observation

ROS reactions and lipid peroxidation play a pivotal role in the tumorigenic and malignant processes of tumors.[44,45] To demonstrate that the accumulation of ROS induced by SC@Lip can exacerbate lipid peroxidation damage in cells, we employed the lipid peroxidation probe BDP 581/591C11 to investigate the lipid peroxidation level in 4T1 cells. As depicted in the CLSM image in Figure 6A, the Sora@Lip group and the SC@Lip group exhibited only a weak green fluorescence signal. However, while the green fluorescence intensity in the Ce6@Lip + US group gradually increased, the cells treated with SC@Lip + US displayed the most intense oxidized green fluorescence of the lipid peroxidation probe BDP 581/591C11, suggesting a significant accumulation of lipid peroxides within the cells. This accumulation of lipid peroxidation damage is detrimental to tumor cells and correlates with tumor malignancy.[46,47] According to the literature, Sorafenib can inhibit the activity of System xc^-.[48,49] System xc^- is widely distributed in the phospholipid bilayer[24] and functions as a crucial component of the cellular antioxidant system. It consists of a heterodimer formed by two subunits, SLC7A11 and SLC3A2. Cystine (Cys-Cys) and glutamic acid are exchanged in and out of the cell at a 1:1 ratio through System xc^-, and the absorbed cystine is then reduced to cysteine (Cys) within the cell, which subsequently participates in the synthesis of glutathione (GSH).[25] Inhibition of System xc^- activity affects GSH synthesis by blocking cystine absorption, leading to a decrease in cellular antioxidant capacity and accumulation of lipid peroxidation.[50]

SLC7A11 expression is directly proportional to the intracellular cystine level, making it one of the key regulators of lipid oxidative damage by controlling cystine influx and GSH biosynthesis.[28,51] Researchers have found that the expression level of SLC7A11 determines the sensitivity of cancer cells to oxidative stress.[28] Overexpression of SLC7A11 can promote the accumulation of disulfide compounds such as cystine in cells, inducing disulfide stress and subsequent cell death, a process known as disulfidptosis.[12,28] The aforementioned theories motivate us to further investigate the SLC7A11 protein expression level and actin cytoskeleton dynamics in cells treated with nanoliposomes. As evident from the CLSM images (Figure 6B), while all groups display expression of the red fluorescently labeled SLC7A11 protein, sonodynamic therapy (Ce6@Lip + US group, SC@Lip + US group) exhibit brighter red fluorescence, indicating levels of SLC7A11 protein expression elevated in these cells. This suggests more accumulation of cystine disulfide within the cells. A high-level cystine environment or SLC7A11 expression increases the sensitivity of glutamine inhibitor to TCA cycle anaplerosis.

The Actin-Tracker Green-488 probe is a fluorescent dye Alexa Fluor 488-labeled phalloidin, namely phalloidin-Alexa Fluor 488, which can specifically bind to filamentous actin (F-actin) in cells, thereby preventing the depolymerization of actin. By utilizing the biological characteristic of phalloidin to stabilize microfilaments, fluorescent dye-labeled phalloidin can display the morphology and distribution of microfilaments in cells. When combined with Phalloidin staining, we observe that in control cells, healthy actin filaments (F-actin) are primarily located in the cell cortex and stress fibers. However, the SC@Lip + US group induces notable changes in cell morphology, characterized by cell contraction and F-actin condensation. Co-staining of SLC7A11 (red) and F-actin (green) reveals that in the SC@Lip + US group, where SLC7A11 is overexpressed, the cytoskeleton network of F-actin collapses, resulting in the inability to maintain cellular homeostasis.

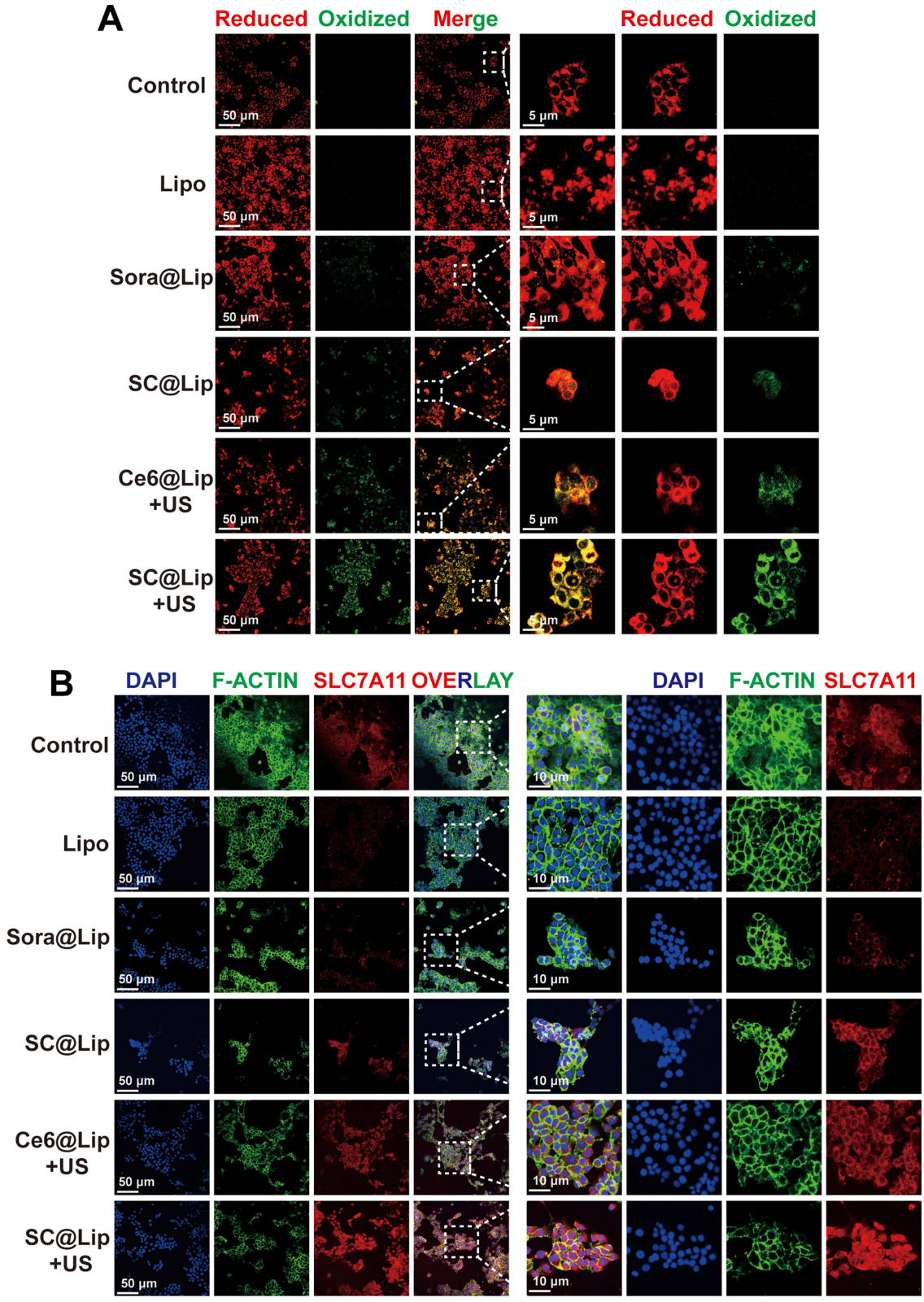

Figure 6 SC@Lip mediates SDT triggered intracellular lipid peroxidation damage and disulfide-like death. (**A**) CSLM images of lipid peroxide after treatment of 4T1 cells with each group. (scale bar: 50μm, 5μm). (**B**) After 4T1 cells treated by each group, the cells were stained with anti-SLC7A11 antibody labeled with Alexa Fluor 555, F-actin was stained with Alexa Fluor 488-labeled phalloidin, and the nucleus was stained with DAPI. (scale bar: 50μm, 10μm). All experiments were repeated independently at least twice, and the results were similar.

Based on these findings, we conclude that SC@Lip under ultrasonic irradiation can induce lipid peroxidation damage in cancer cells, leading to high uptake of cystine, abnormal disulfide bond formation in actin cytoskeleton proteins, and the collapse of the actin network. This ultimately results in disulfide stress and subsequent disulfidptosis, explaining the superior anticancer effect mediated by SC@Lip in sonodynamic therapy. These insights provide a theoretical foundation for subsequent in vivo treatment experiments.

Antitumor Efficacy of SC@Lip Mediated SDT in vivo

Given the toxicity of lipid peroxidation damage and disulfide-like death effect exhibited by SC@Lip in vitro, we subsequently evaluated the potential of sonodynamic therapy (SDT) for anti-cancer treatment in a mouse model of 4T1 subcutaneous tumor. The treatment cycle is schematically depicted in Figure 7A.

Initially, 30 Balb/c mice with 4T1 tumors (approximately 100 mm^3) were randomly divided into five groups and administered the following treatments: I) PBS (Control); II) Sora@Lip; III) SC@Lip; IV) Ce6@Lip + US; V) SC@Lip + US. Mice in groups II to V received intravenous injections of different liposomes at the same nanoliposome dose (10 mg kg^{-1}) on days 0, 3, and 7. Additionally, mice in groups IV and V received ultrasonic irradiation (2 W/cm^2, 3 min) on days 1, 4, and 7.

As seen from the tumor volume growth curve (Figure 7B), tumors in the control group grew rapidly. Sora@Lip, SC@Lip, and Ce6@Lip + US showed similar tumor growth trends with only limited tumor inhibition. The median survival times were 21, 22, and 25 days, respectively, slightly longer than those of untreated mice (Figure 7D). However, SC@Lip + US exhibited the best therapeutic effect on 4T1 tumors, with relatively slow tumor growth and a median survival time of 30 days, outperforming other treatment groups. Notably, no significant weight changes were observed in any of the treatment groups (Figure 7C).

To further assess the therapeutic efficacy, we collected tumors for pathological diagnosis tests, including H&E staining, SLC7A11 protein expression analysis, TUNEL staining, and PCNA staining. As depicted in Figure 7E, the SC@Lip + US group exhibited extensive tumor cell necrosis, which was more pronounced than in the other groups. Interestingly, the SC@Lip + US group also displayed the highest expression of SLC7A11 protein, consistent with the extensive necrosis observed in the H&E staining. Those phenomena suggest that cancer cells with high SLC7A11 expression may be more vulnerable to oxidative stress, ultimately leading to cancer cell death. TUNEL staining (green fluorescence) further confirmed that SC@Lip + US induced extensive apoptosis of cancer cells, while PCNA staining (red fluorescence) indicated a decrease in the tumor's proliferation index following treatment. In summary, these results demonstrate that the SDT effect mediated by SC@Lip has therapeutic impact on the tumor-bearing mouse model, with no apparent side effects.

Biological Safety Analysis of SC@Lip

To assess the in vivo administration, we performed a hemolysis test (Figure 8A), which revealed that SC@Lip did not induce hemolysis at concentrations of 500 μg/mL or 1 mg/mL, thereby confirming its excellent blood compatibility. Subsequently, we evaluated the biological safety and biocompatibility of SC@Lip, which is crucial for its clinical translation. We administered SC@Lip to healthy mice and collected blood samples at days 1, 3, 7, 14, and 21 for biochemical examination and blood cell analysis, using untreated healthy mice as the control group. As shown in Figure 8B, the fluctuations of blood indices across the biochemical groups were negligible, demonstrating the high safety profile of SC@Lip. Furthermore, we collected the primary organs of the mice, including the heart, liver, spleen, lungs, and kidneys, and performed pathological H&E staining (Figure 8D). No significant pathological changes were observed, further validating the potential of SC@Lip for clinical applications.

Biological Distribution of Liposomes of SC@Lip

SC@Lips were injected into Balb/c tumor-bearing mice, Ce6 fluorescence began to accumulate at the tumor site at 8 h post-injection, reached a peak at 24 h post-injection, and then declined at 30 h post-injection (Figure 8C). SC@lips mainly distributed in liver and spleen, followed by tumor sites. For those results, we chose to perform ultrasound irradiation 24 hours after injection.

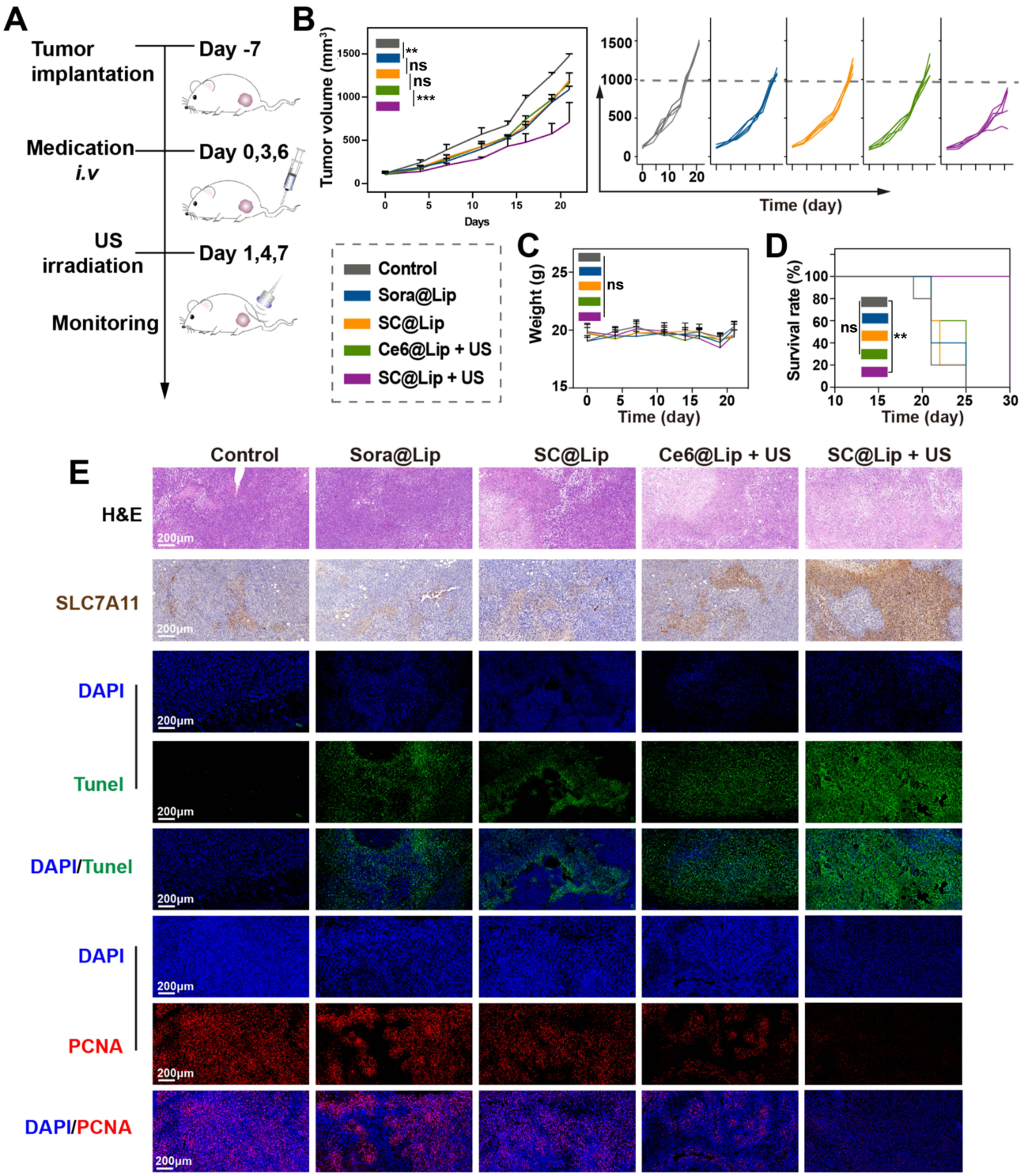

Figure 7 Antitumor efficacy of SC@Lip mediated SDT in vivo. (**A**) The therapeutic schematic diagram for 4T1 subcutaneous tumor model. (**B**) The subcutaneous tumor volume growth curve of treatment groups and the tumor volume growth curve of a single mouse in each treatment group. (**C**) Weight curve of mice in each group during the treatment period. (**D**) Survival curve of mice in each group. (**E**) H&E staining, SLC7A11 IHC, TUNEL staining and PCNA staining of tumor tissues from different groups. (scale bar: 200μm).(**ns** means no statistical difference, **p < 0.01, ***p < 0.001).

Conclusion

In summary, our work presents an anticancer system utilizing an SDT lipid sonosensitizer, which aims to achieve a synergistic anticancer effect through SDT and trigger disulfidptosis-like cell death. This approach differs from conventional therapies that induce tumor cell apoptosis. As a proof of concept, we constructed artificial biofilm

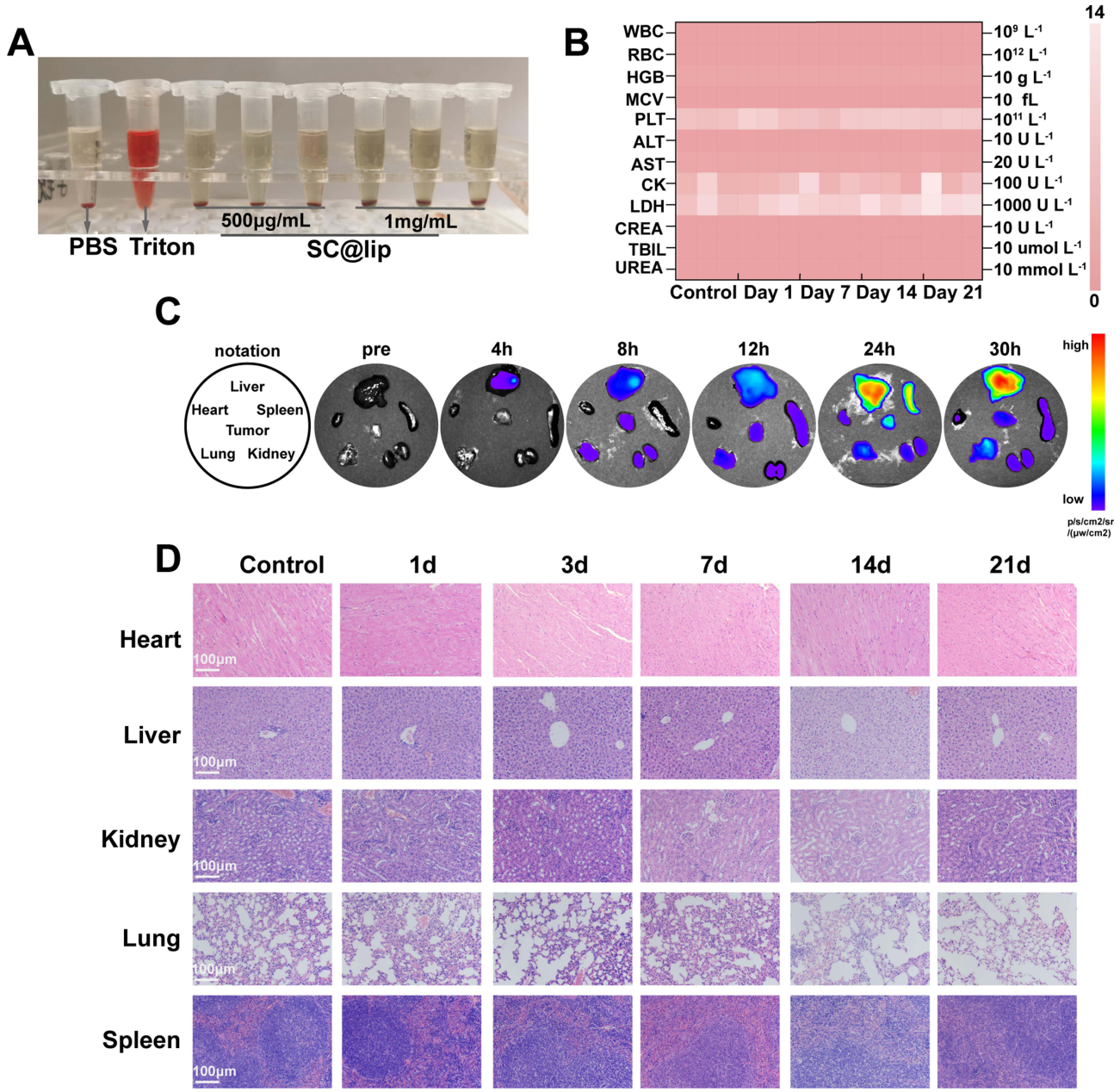

Figure 8 Biological safety analysis of SC@Lip. (**A**) Hemolysis experiment of SC@Lip. (**B**) Blood biochemical test of healthy mice treated with SC@Lip. (**C**) Fluorescence images of ex vivo tissues (tunor, heart, liver, kidneys, lung and spleen) at different time points. (**D**) The main organs H&E stain of healthy mice treated with SC@Lip (scale bar: 100μm).

nanoliposomes by combining Ce6 and Sorafenib. In the tumor microenvironment, SC@Lip generates sufficient ROS under ultrasound (US) irradiation, inducing a large number of lipid peroxide (LPO) formaation in cells, which leads to a substantial increase in the expression of SLC7A11 protein in cancer cells and promotes the accumulation of disulfide-ralated stress. Concurrently, intracellular reducting substances such as glutathione (GSH) and NADPH are overconsumed. This results in the inability of the cells to transport cystine, causing the accumulation of disulfide and ultimately leading to disulfidptosis. These two mechanisms synergistically enhance the SDT anticancer effect, triggering disulfidptosis-like cell death and achieving anti-tumor efficacy both in vitro and in vivo. Consequently, SC@Lip is poised to become an effective SDT sonosensitizer for inducing disulfidptosis. Our findings offer a promising strategy for future research on nano-liposomes as anticancer sonosensitizers.

Abbreviations

Ce6, Chlorin e6; CHOL, Cholesterol; CLSM, Confocal laser scanning microscopy; Calcein-AM, Calcein acetoxymethyl ester; Cystine, Cys-Cys; cysteine, Cys; DCFH-DA, 2',7'-dichlorodihydrofluorescein diacetate; DPBF, 1, 3-diphenylisopropylfuran; DPPC, 1.2-dipalmitoyl-sn-glycero-3-phosphocholine; DSPE-mPEG2000, 1.2-distearoyl-sn-glycero-3-phosphoethanolamine-N-[methoxy(polyethylene glycol)-2000]; FCM, Flow cytometer; GSH, Glutathione; H&E, Hematoxylin and eosin; HPLC, High efficiency liquid chromatography; Lipo, Liposomes; LPO, Lipid peroxidation; NADPH, Nicotinamide adenine dinucleotide phosphate; PCNA, Proliferating cell nuclear antigen; PFH, Perfluorohexane; PI, Propidium iodide; ROS, Reactive oxygen species; SDT, Sonodynamic therapy; SLC7A11(xCT-), Solute carrier family 7 member 11; Sora, Sorafenib; SOSG, Singlet oxygen sensor green fluorescent probe; TEM, Transmission electron microscopy; TUNEL, TdT-mediated dUTP nick end labeling; US, Ultrasound.

Data Sharing Statement

All data generated or analyzed during this study are included in this published article and its Supplementary Information Files.

Ethics Approval and Informed Consent

All animal experiments were approved by the Animal Ethics Committee of Chongqing medical University and were conducted in compliance with the National Institutes of Health guide for the care and use of Laboratory animals animal welfare ethics (acceptance number: IAUC-CQMU-2024-0016), as well as the internationally recognized `3Rs" principles of animal experiments.

Consent for Publication

All authors agreed to publish this manuscript.

Author Contributions

All authors made a significant contribution to the work reported, whether that is in the conception, study design, execution, acquisition of data, analysis and interpretation, or in all these areas; took part in drafting, revising or critically reviewing the article. Specifically, Hongwei Xiang and Bin Shen made the first and equal contributions. Chunmei Zhang, while in a secondary role, also made significant contributions. The entire study was conducted under the supervision and guidance of Professor Rui Li, with funding support. All authors gave final approval of the version to be published; have agreed on the journal to which the article has been submitted; and agree to be accountable for all aspects of the work.

Funding

This study was supported by the Chongqing Talent Plan (cstc2021ycjh-bgzxm0077).

Disclosure

The authors declare that they have no competing interests in this work.

References

1. Bertheloot D, Latz E, Franklin BS. Necroptosis, pyroptosis and apoptosis: An intricate game of cell death. *Cell Mol Immunol*. 2021;18(5):1106–1121.
2. Zhang C, Liu X, Jin S, Chen Y, Guo R. Ferroptosis in cancer therapy: A novel approach to reversing drug resistance. *Mol Cancer*. 2022;21(1):47. doi:10.1186/s12943-022-01530-y
3. Yu P, Zhang X, Liu N, Tang L, Peng C, Chen X. Pyroptosis: Mechanisms and diseases. *Signal Transduct Target Ther*. 2021;6(1):128. doi:10.1038/s41392-021-00507-5
4. Carneiro BA, El-Deiry WS. Targeting apoptosis in cancer therapy. *Nat Rev Clin Oncol*. 2020;17(7):395–417. doi:10.1038/s41571-020-0341-y
5. Zheng T, Liu Q, Xing F, Zeng C, Wang W. Disulfidptosis: A new form of programmed cell death. *J Exp Clin Cancer Res*. 2023;42(1):137. doi:10.1186/s13046-023-02712-2
6. Hadian K, Stockwell BR. The therapeutic potential of targeting regulated non-apoptotic cell death. *Nat Rev Drug Discov*. 2023;22(9):723–742. doi:10.1038/s41573-023-00749-8

7. Machesky LM. Deadly actin collapse by disulfidptosis. *Nat Cell Biol*. 2023;25(3):375–376. doi:10.1038/s41556-023-01100-4
8. Hecht F, Zocchi M, Alimohammadi F, Harris IS. Regulation of antioxidants in cancer. *Mol Cell*. 2024;84(1):23–33. doi:10.1016/j.molcel.2023.11.001
9. Liu X, Nie L, Zhang Y, et al. Actin cytoskeleton vulnerability to disulfide stress mediates disulfidptosis. *Nat Cell Biol*. 2023;25(3):404–414. doi:10.1038/s41556-023-01091-2
10. Hogg PJ. Targeting allosteric disulphide bonds in cancer. *Nat Rev Cancer*. 2013;13(6):425–431. doi:10.1038/nrc3519
11. DeMartino AW, Zigler DF, Fukuto JM, Ford PC. Carbon disulfide. Just toxic or also bioregulatory and/or therapeutic? *Chem Soc Rev*. 2017;46(1):21–39. doi:10.1039/C6CS00585C
12. Zhao D, Meng Y, Dian Y, et al. Molecular landmarks of tumor disulfidptosis across cancer types to promote disulfidptosis-target therapy. *Redox Biol*. 2023;68:102966. doi:10.1016/j.redox.2023.102966
13. Trachootham D, Alexandre J, Huang P. Targeting cancer cells by ROS-mediated mechanisms: A radical therapeutic approach? *Nat Rev Drug Discov*. 2009;8(7):579–591. doi:10.1038/nrd2803
14. Jia C, Guo Y, Wu FG. Chemodynamic therapy via Fenton and Fenton-like nanomaterials: Strategies and recent advances. *Small*. 2022;18(6):e2103868. doi:10.1002/smll.202103868
15. Liu Y, Bhattarai P, Dai Z, Chen X. Photothermal therapy and photoacoustic imaging via nanotheranostics in fighting cancer. *Chem Soc Rev*. 2019;48(7):2053–2108. doi:10.1039/c8cs00618k
16. Son S, Kim JH, Wang X, et al. Multifunctional sonosensitizers in sonodynamic cancer therapy. *Chem Soc Rev*. 2020;49(11):3244–3261. doi:10.1039/C9CS00648F
17. Lin X, Song J, Chen X, Yang H. Ultrasound-activated sensitizers and applications. *Angew Chem Int Ed Engl*. 2020;59(34):14212–14233. doi:10.1002/anie.201906823
18. Liang S, Yao J, Liu D, Rao L, Chen X, Wang Z. Harnessing nanomaterials for cancer sonodynamic immunotherapy. *Adv Mater*. 2023;35(33):e2211130. doi:10.1002/adma.202211130
19. Mitchell MJ, Billingsley MM, Haley RM, Wechsler ME, Peppas NA, Langer R. Engineering precision nanoparticles for drug delivery. *Nat Rev Drug Discov*. 2021;20(2):101–124. doi:10.1038/s41573-020-0090-8
20. Fan D, Cao Y, Cao M, Wang Y, Cao Y, Gong T. Nanomedicine in cancer therapy. *Signal Transduct Target Ther*. 2023;8(1):293. doi:10.1038/s41392-023-01536-y
21. Cheng Z, Li M, Dey R, Chen Y. Nanomaterials for cancer therapy: Current progress and perspectives. *J Hematol Oncol*. 2021;14(1):85. doi:10.1186/s13045-021-01096-0
22. Zhang Y, Zhang X, Yang H, et al. Advanced biotechnology-assisted precise sonodynamic therapy. *Chem Soc Rev*. 2021;50(20):11227–11248. doi:10.1039/D1CS00403D
23. Aboushousha R, van der Velden J, Hamilton N, et al. Glutaredoxin attenuates glutathione levels via deglutathionylation of Otub1 and subsequent destabilization of system xC. *Sci Adv*. 2023;9(37):eadi5192. doi:10.1126/sciadv.adi5192
24. Bridges R, Lutgen V, Lobner D, Baker DA. Thinking outside the cleft to understand synaptic activity: Contribution of the cystine-glutamate antiporter (system xc-) to normal and pathological glutamatergic signaling. *Pharmacol Rev*. 2012;64(3):780–802. doi:10.1124/pr.110.003889
25. Parker JL, Deme JC, Kolokouris D, et al. Molecular basis for redox control by the human cystine/glutamate antiporter system xc. *Nat Commun*. 2021;12(1):7147. doi:10.1038/s41467-021-27414-1
26. Liu X, Olszewski K, Zhang Y, et al. Cystine transporter regulation of pentose phosphate pathway dependency and disulfide stress exposes a targetable metabolic vulnerability in cancer. *Nat Cell Biol*. 2020;22(4):476–486. doi:10.1038/s41556-020-0496-x
27. He F, Zhang P, Liu J, et al. ATF4 suppresses hepatocarcinogenesis by inducing SLC7A11 (xCT) to block stress-related ferroptosis. *J Hepatol*. 2023;79(2):362–377. doi:10.1016/j.jhep.2023.03.016
28. Yan Y, Teng H, Hang Q, et al. SLC7A11 expression level dictates differential responses to oxidative stress in cancer cells. *Nat Commun*. 2023;14(1):3673. doi:10.1038/s41467-023-39401-9
29. Hayes JD, Dinkova-Kostova AT, Tew KD. Oxidative stress in cancer. *Cancer Cell*. 2020;38(2):167–197. doi:10.1016/j.ccell.2020.06.001
30. Gorrini C, Harris IS, Mak TW. Modulation of oxidative stress as an anticancer strategy. *Nat Rev Drug Discov*. 2013;12(12):931–947. doi:10.1038/nrd4002
31. Tang W, Chen Z, Zhang W, et al. The mechanisms of sorafenib resistance in hepatocellular carcinoma: Theoretical basis and therapeutic aspects. *Signal Transduct Target Ther*. 2020;5(1):87. doi:10.1038/s41392-020-0187-x
32. Cabanillas ME, Ryder M, Jimenez C. Targeted therapy for advanced thyroid cancer: Kinase inhibitors and beyond. *Endocr Rev*. 2019;40(6):1573–1604. doi:10.1210/er.2019-00007
33. Nie T, Zou W, Meng Z, et al. Bioactive iridium nanoclusters with glutathione depletion ability for enhanced sonodynamic-triggered ferroptosis-like cancer cell death. *Adv Mater*. 2022;34(45):e2206286. doi:10.1002/adma.202206286
34. Cai H, Tan P, Chen X, et al. Stimuli-sensitive linear-dendritic block copolymer-drug prodrug as a nanoplatform for tumor combination therapy. *Adv Mater*. 2022;34(8):e2108049. doi:10.1002/adma.202108049
35. Sun D, Zhou S, Gao W. What went wrong with anticancer nanomedicine design and how to make it right. *ACS Nano*. 2020;14(10):12281–12290. doi:10.1021/acsnano.9b09713
36. Lahooti B, Akwii RG, Zahra FT, et al. Targeting endothelial permeability in the EPR effect. *J Control Release*. 2023;361:212–235. doi:10.1016/j.jconrel.2023.07.039
37. Ikeda-Imafuku M, Wang L Li-Wen, Rodrigues D, Shaha S, Zhao Z, Mitragotri S. (2022). Strategies to improve the EPR effect: A mechanistic perspective and clinical translation. J Control Release, 345 512–536. 10.1016/j.jconrel.2022.03.043
38. Żamojć K, Zdrowowicz M, Rudnicki-Velasquez PB, et al. The development of 1,3-diphenylisobenzofuran as a highly selective probe for the detection and quantitative determination of hydrogen peroxide. *Free Radic Res*. 2017;51(1):38–46. doi:10.1080/10715762.2016.1262541
39. Gollmer A, Arnbjerg J, Blaikie FH, et al. Singlet oxygen sensor green®: Photochemical behavior in solution and in a mammalian cell. *Photochem Photobiol*. 2011;87(3):671–679. doi:10.1111/j.1751-1097.2011.00900.x
40. Meng Y, Niu X, Li G. Liposome nanoparticles as a novel drug Delivery system for therapeutic and diagnostic applications. *Curr Drug Deliv*. 2022;20(1):41–56. doi:10.2174/1567201819666220324093821

41. Song X, Zhang Q, Chang M, et al. Nanomedicine-enabled sonomechanical, sonopiezoelectric, sonodynamic, and sonothermal therapy. *Adv Mater*. 2023;35(31):e2212259. doi:10.1002/adma.202212259
42. Forman HJ, Zhang H. Targeting oxidative stress in disease: Promise and limitations of antioxidant therapy. *Nat Rev Drug Discov*. 2021;20 (9):689–709. doi:10.1038/s41573-021-00233-1
43. Xiong Y, Xiao C, Li Z, Yang X. Engineering nanomedicine for glutathione depletion-augmented cancer therapy. *Chem Soc Rev*. 2021;50 (10):6013–6041. doi:10.1039/D0CS00718H
44. Jiang X, Stockwell BR, Conrad M. Ferroptosis: Mechanisms, biology and role in disease. *Nat Rev Mol Cell Biol*. 2021;22(4):266–282. doi:10.1038/s41580-020-00324-8
45. Cheung EC, Vousden KH. The role of ROS in tumour development and progression. *Nat Rev Cancer*. 2022;22(5):280–297. doi:10.1038/s41568-021-00435-0
46. Martin-Perez M, Urdiroz-Urricelqui U, Bigas C, Benitah SA. The role of lipids in cancer progression and metastasis. *Cell Metab*. 2022;34 (11):1675–1699. doi:10.1016/j.cmet.2022.09.023
47. Martínez-Reyes I, Chandel NS. Cancer metabolism: Looking forward. *Nat Rev Cancer*. 2021;21(10):669–680. doi:10.1038/s41568-021-00378-6
48. Chen X, Kang R, Kroemer G, Tang D. Broadening horizons: The role of ferroptosis in cancer. *Nat Rev Clin Oncol*. 2021;18(5):280–296. doi:10.1038/s41571-020-00462-0
49. Bejjani AC, Finn RS. Hepatocellular carcinoma: Pick the winner-tyrosine kinase inhibitor versus immuno-oncology agent-based combinations. *J Clin Oncol*. 2022;40(24):2763–2773. doi:10.1200/JCO.21.02605
50. Zhang HF, Klein Geltink RI, Parker SJ, Sorensen PH. Transsulfuration, minor player or crucial for cysteine homeostasis in cancer. *Trends Cell Biol*. 2022;32(9):800–814. doi:10.1016/j.tcb.2022.02.009
51. Lei G, Zhuang L, Gan B. Targeting ferroptosis as a vulnerability in cancer. *Nat Rev Cancer*. 2022;22(7):381–396. doi:10.1038/s41568-022-00459-0